15TH IEA HEAT PUMP CONFERENCE
MAY 26–29, 2026 | HOFBURG
VIENNA 2026
DECARBONISATION THROUGH INNOVATION

Waste Heat Recovery Using A Miniaturized Heat Pump at Mobile Base Stations

Tianhao Xu, Hatef Madani

Department of Energy Technology, KTH Royal Institute of Technology, 100 44 Stockholm, Sweden

Abstract

The widespread 5G telecommunication base stations (TBS) represent a widely distributed waste heat resource in urban areas which is yet unexploited. The low-grade waste heat at 30–45°C within TBS cabinets coincides with year-round building heat demands for Domestic Hot Water (DHW) circulation systems. The need for temperature upgrade and strict volume constraints of TBS cabinets create a critical research and development need for miniaturized, cabinet-integrated heat pump (HP) solutions. This paper presents a comprehensive "concept-to-deployment" investigation of such a waste heat recovery system based on a miniaturized heat pump. In this paper, we designed and prototyped a novel, cabinet-integrated "miniaturized heat pump door" using R600a charge below 150 g. Through a dedicated test rig, we performed experimental characterization of HP performance and used experimental data to validate a numerical thermodynamic (IMST-ART) model of the HP. Experimental results show that the prototype successfully upgraded cabinet's warm air at 37 °C to DHW at 55 °C with a total COP of 3.1 and waste heat recovery ratio of 85%. We used the validated HP model to investigate improved evaporator alternatives with denser fins and a microchannel heat exchanger. Through combined thermodynamic and heat transfer simulation, we identified an HP and cabinet renovation delivering 1.45 kW of heat to DHW systems while ensuring critical electronics hotspot junction temperatures remained safely below 60°C. The techno-economic analysis of the integrated system shows that the heating costs can be saved by 858 €/year through reduced district heating demands for DHW production, considering the current energy prices in Sweden. This saving justifies a capital investment of 10,000 € for seven-year operation while HP components cost only 2,000 € at our laboratory. The experimental and simulation results in this paper validate a novel and viable waste heat recovery pathway to valorize waste heat from telecommunication infrastructure.

Keywords: Waste Heat Recovery; Miniaturized Heat Pump; Domestic Hot Water; Experimental Investigation; Sector Coupling

1. Introduction

The deployment of 5G networks is accelerating worldwide, leading to a substantial rise in the energy use of the Information and Communication Technology (ICT) sector. More than 70% of this energy is consumed by the Radio Access Network (RAN), particularly at telecommunication base stations (TBS), where electronic units such as the Baseband Unit (BBU) and Power Supply Unit (PSU) convert most of their electrical power into low-grade waste heat inside outdoor cabinets [1-3]. With millions of TBS cabinets installed globally—and several thousand in cities such as Stockholm alone—this waste heat constitutes a highly distributed but almost entirely unexploited heat resource.

In Nordic countries such as Sweden, this situation aligns with the year-round heat demand of domestic hot water (DHW) circulation systems in commercial and multifamily residential buildings. Because many rooftop TBS are located only a few meters from the hydronic loops, direct coupling between the waste heat source and building heating demand is technically feasible. The internal cabinet air temperature typically ranges from 30–45 °C [4], below the required DHW circulation temperatures (>50 °C) due to legionella prevention regulations [5]. This means heat-pump (HP) solutions are needed for recovering such low-grade waste heat.

However, current thermal management systems for TBS cabinets are not designed for this purpose. Existing cabinet-cooling systems, such as air-to-air heat exchangers, fan-assisted ventilation, heat-pipe systems, and hybrid vapor-compression coolers, are designed solely for equipment cooling and reject all heat to ambient [6-

15th IEA Heat Pump Conference 2026 - BRE4.1 - https://doi.org/10.23697/zdy6-c710

7]. On the other hand, while the application of waste-heat recovery is well documented for large, centralized sources like data centers in Stockholm and London [8-9], these solutions cannot be directly applied to TBS cabinets because of the drastic difference in thermal scale and integration constraints. The recovery of heat from smaller, distributed sources like rooftop TBS requires a highly miniaturized, cabinet-integrated system, which is not yet available in literature or in real deployments.

To fully assess the feasibility of TBS waste-heat recovery, this paper presents a comprehensive investigation including hardware design, prototyping and testing, heat-transfer and thermodynamic analyses, and economic evaluation of integrating a heat pump with building DHW circulation systems. Using combined experimental and numerical methods, this study demonstrates how an experimentally validated miniaturized HP can establish an economically feasible pathway for waste-heat recovery from mobile base stations. Feasible realization of this concept can support the transition toward more sustainable urban energy and telecommunication infrastructures.

2. Methods

2.1. Prototyping and Experimental Investigations

Figure 1 shows the miniaturized heat recovery heat pump realized in our laboratory, functioning as a “heat pump door” to the TBS cabinet replacing its original air-to-air heat exchanger. As shown in Figure 1 (b-c), the HP components are integrated directly into the door frame, with sealing applied to prevent internal air leakage. Hoses connected to the condenser and electrical cables are led through a manhole at the lower position of door. Inside the cabinet, we deployed dummy BBU and PSU units embedded with foil resistive heaters to emulate heat dissipation.

Figure 1. Prototyped miniaturized heat pump: (a) heat pump components; (b) heat pump installed as a compartment of cabinet’s door; (c) heat pump integrated with cabinet.

Table 1 lists the major technical parameters of the heat pump components, which are off-the-shelf commercial products. These components were selected to form a compact assembly due to the strict volume limitation. The heat pump prototype uses R600a as the refrigerant with a charge below 150 g.

Table 1 Components of the heat pump prototype

Component	Type	Key Technical Parameters
Compressor	Scroll compressor	Swept volume: 15 cc; variable speed: 700-5000 RPM
Condenser	Brazed plate heat exchanger	Number of plates: 28; Dimensions: 89×74×210 mm
Evaporator	Finned coil heat exchanger	Fin spacing: 4.3 mm; circuit volume:0.45 dm^3; external surface area: 2.0 m^2
Expansion device	Electric expansion valve	Maximum refrigerating capacity: 2 kW

As shown in Figure 2, a dedicated test rig was constructed to investigate the HP's performance under emulated TBS thermal loads and operating conditions. The system was heavily instrumented with calibrated T-type thermocouples (measurement error: $\pm$0.1 K) to measure air, water, and refrigerant temperatures at all critical points (e.g., BBU/HP inlets/outlets, compressor suction/discharge). Refrigerant pressures were recorded with high- and low-pressure transducers, water flow rate with a magnetic flow meter, and the electrical consumption of all components (heaters, compressor, BBU fans, HP fans) with digital power meters.

The waste heat load was simulated using foil resistive heaters controlled by a solid-state relay (SSR). The dummy BBU has a form factor of 86 mm (height) × 442 mm (width) × 310 mm (depth). It is a standard 2U chassis cooled by lateral horizontal airflow triggered by three parallel axial DC fans.

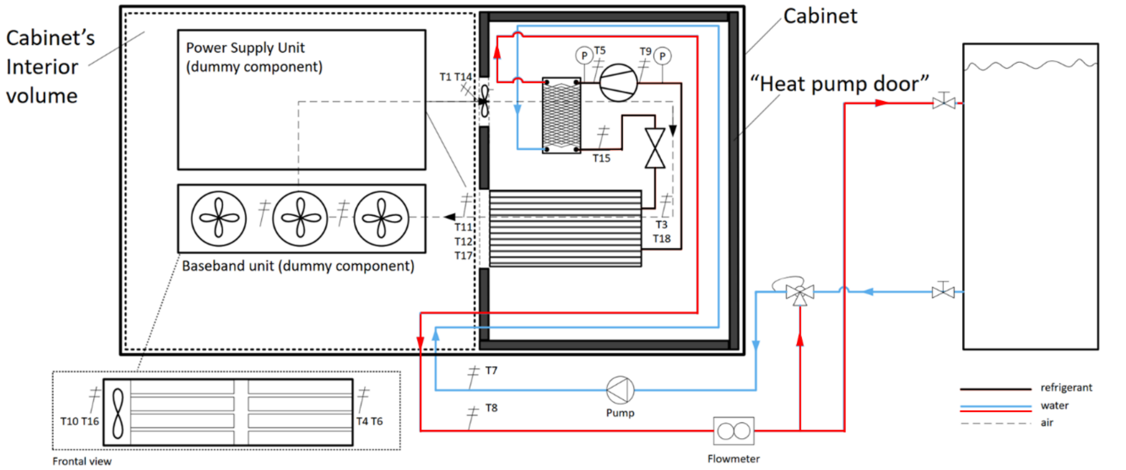

Figure 2. Schematics of the test rig for investigating heat recovery performance of the heat pump (Lateral view).

Key performance indicators such as COPs were calculated from the raw measurement data, using the CoolProp library for all fluid thermodynamic properties. The heating capacity of the condenser (Q_{cond}) was calculated by the heat balance on the water side using temperature difference between T8 and T7 as well as volumetric flow rate read by the Magnetic flow meter. We defined compressor-only COP for heating ($COP_{1,comp}$) and total COP for heating ($COP_{1,tot}$) according to Eqs.(1-2). In Eq. (2), the compressor power and fan power were read by the Yokogawa and Carlo Gavazzi power meters, respectively.

Table 2 lists the measurement uncertainty for each instrument. Based on this information, uncertainty analyses were performed using the root-sum-square method accounting for both relative reading errors and absolute range-based errors. Measurement uncertainty analyses show that the expanded uncertainty at a 95% confidence level of Q_{cond} and COPs is $\pm$4.2%. that of saturation pressure is $\pm$0.35 K. Furthermore, the uncertainty of the saturation pressure, when propagated through the refrigerant state equations, corresponds to an equivalent saturation temperature uncertainty of 0.35 K.

Table 2 Specifications of measurement instruments

Measurement Device	**Type**	**Quantity**	**Precision**
Thermocouple	T-type (calibrated)	18	±0.1 °C
Pressure transducer	Danfoss DSTP110	2	±1% of full scale (high pressure range: 0-30 bar; low pressure range: 0-10 bar)
Magnetic flow meter	Yokogawa AXF005G	1	±0.35% of read flow rate
Digital power meter	Yokogawa WT130	1	±(0.15% of read power + 0.1% of measurement range)
	Carlo Gavazzi VMUXUS1X	1	±1.0% of read power

$$COP_{1,comp} = \frac{Q_{cond}}{W_{comp}} \tag{1}$$

$$COP_{1,tot} = \frac{Q_{cond}}{W_{comp} + W_{pump} + W_{fan,HP}} \tag{2}$$

The cooling capacity of HP (Q_{evap}) is obtained from the refrigerant-side energy balance, see Eq. (3). The corresponding air-side volumetric flow rate is calculated using Eq. (4). Here, $V_{a,HP}$ is derived from the heat balance of sensible heat capacity of air. The air inlet temperature ($T_{a,in,HP}$) is the average value of temperature measurements of T1 and T14; the air outlet temperature ($T_{a,out,HP}$) is the average value of temperature measurements of T11, T12 and T17, shown in Figure 2.

$$Q_{evap} = \dot{m}_r \, (h_{suc} - h_{exv,out}) \tag{3}$$

$$V_{a,HP} = \frac{Q_{evap}}{\rho_a c_{p,a} (T_{a,in,HP} - T_{a,out,HP})} \tag{4}$$

The heat recovery ratio (HRR) was calculated to quantify the effectiveness of waste heat capture, defined as the ratio of heat produced by the condenser to the total electrical power supplied to the heaters $Q_{heaters}$ and two sets of fans, which are eventually converted to heat gains inside the cabinet.

$$HRR = \frac{Q_{cond}}{Q_{heaters} + W_{fan,HP} + W_{fan,BBU}} \tag{5}$$

2.2. Numerical simulations of HP and temperatures in cabinet

The heat pump cycle was simulated using the IMST-ART software (v4.10), which is a commercially available steady-state vapor-compression modelling tool widely used for performance prediction of heat pump and refrigeration systems [10]. The heat pump components were configured with internal IMST models using manufacturer catalogue information. The program solves the cycle iteratively until mass and energy balances converge within a tolerance of 0.1%. The outputs include COP, heating capacity, compressor power, refrigerant mass flow rate, and all thermodynamic state variables. When performing model validation with experimental data, the measured temperatures of secondary fluids, superheat, and subcooling were set as input values in the model.

When replacing the original cabinet cooling with a heat pump, it is not enough to predict only the air temperature at the evaporator outlet. The internal electronic performance and reliability of BBU can be evaluated by two key temperatures: the average printed circuit board temperature ($T_{\mathrm{PCB,avg}}$) and the junction hotspot temperature (T_j). In this work, we firstly modelled the BBU as a lumped heat source with total dissipation Q_{BBU}, exchanging heat with the internal airflow via an effective overall heat-transfer coefficient UA_{BBU}. The PCB–air temperature difference is therefore expressed as Eq.(6).

$$T_{PCB,avg} - T_{air,avg} = \frac{Q_{BBU}}{UA_{BBU}} \tag{6}$$

As commonly done in electronics cooling, UA_{BBU} is correlated to the forced-convection heat-transfer coefficient h, which follows well-established power-law scaling with air velocity based on classical correlations such as Dittus–Boelter or Churchill–Bernstein [11-12]. V_{BBU} is the air flowrate through the lateral cross-section of the BBU for cooling the PCBs.

$$h \propto v^{0.8} \Rightarrow UA_{BBU} = UA_{ref} (\frac{V_{BBU}}{V_{ref}})^{0.8} \tag{7}$$

UA_{ref} is calibrated using a measured reference operating point for a real 2U server whose heating capacity of 700 W was cooled with an airflow of 170-343 CFM [13].

The hotspot junction temperature T_j of key components is calculated using the classical junction-to-ambient resistance stack, see Eq.(8), where P_{hot} is the local heat dissipation capacity of the hotspot component. Empirical studies of forced-convection electronics cooling report that R_{j-a} typically decreases with airflow following a power law $R_{j-a} \propto v^{-n}$ with $n \approx 0.3 - 0.4$ [14]. According to [15], a typical anchoring value for reference R_{j-a} is 1.2 K/W at a reference V_{BBU} of 350 CFM ; P_{hot} was set as 25 W. R_{j-a} was adjusted by the actual V_{BBU} according to Eq. (9).

$$T_j = T_{air,avg} + P_{hot} R_{j-a} \tag{8}$$

$$R_{th,j-a}(V_{\mathrm{BBU}}) = R_{th,j-a,\mathrm{\,ref}} (\frac{V_{\mathrm{BBU,\,ref}}}{V_{\mathrm{BBU}}})^{0.36} \tag{9}$$

2.3. Techno-economic evaluation of integration

DHW recirculation (DHWR) loops are standard installations to ensure immediate hot-water delivery and hygienic conditions at all draw-off points [16]. Because the DHWR pump circulates water continuously to maintain the temperature at peripheral taps, DHWR heat losses represent a constant base load throughout the year, especially in new buildings designed for short waiting times. Field studies by BEBO [17] reported that DHWR losses vary between 2.3 and 28 kWh $m^{-2}\cdot yr^{-1}$. Figure 3 illustrates the proposed integration of the HP condenser into DHW circulation systems of a building originally heated by DH. Two short extension pipes link the end bridge near the roof to the condenser, where a three-way diverting valve regulates the water flow through the HP circuit. The HP can compensate the heat loss through the DHW circulation system with a controllable flow enabled by the three-way diverting flow, increasing the return temperature in the DHWR lines to the DH substation so that it requires less amount of heat from the DH. The hot water flow rate in the DHWR circuit is nearly constant and well-suited to the continuous operation of a small-capacity HP.

In this integrated solution, the water flow rate through the heat pump condenser must be stably and appropriately controlled through the three-way diverting valve on the end bridge. Insufficient flow can cause condenser water outlet temperature and discharge temperature to become riskily high. Therefore, the circulation flow rate in DHWR systems must exceed the minimum value required by the heat pump condenser to ensure a suitable temperature lift of water, which is around 0.25 m^3/h (0.07 L/s) according to the heat pump design. The pressure drop across the condenser is as insignificant as 0.32 kPa when the flowrate is set as 0.25 m^3/h.

In the simulation of integrated systems, the boundary conditions summarized in Table 2 are used to define a representative base-case building and DHW circulation system into which the HP-integrated TBS cabinet is virtually coupled. The building is modelled with a conditioned floor area of 2000 m² and a specific DHWR loss of 10 kWh/(m²·year), giving an annual circulation loss of 20 MWh. This loss is converted to a quasi-steady thermal load of approximately 2.3 kW, and the waste heat recovery HP can always partially cover this load. In this way, DH costs can be saved as the heating load is covered by the HP instead.

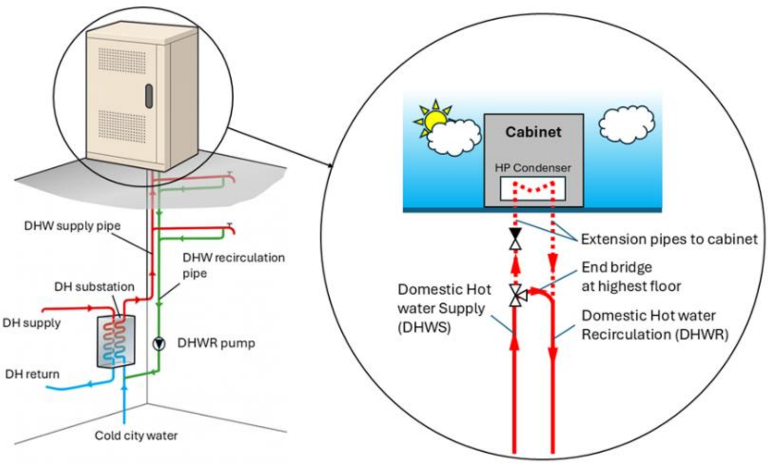

Figure 3. Concept of integration to achieve heat recovery from a HP-integrated TBS cabinet into DHW circulation systems

Table 3 Assumptions of technical and economic boundary conditions for waste heat recovery analyses.

Boundary conditions	Values
Specific DHWR loss per floor area [kWh/m^2]	10
Floor area [m^2]	2000
Circulation flow rate in DHWR system [m^3/h]	0.5
Setpoint of supply and return (recirculation) temperatures at the heat exchanger in original DHW circulation systems [°C]	55/50°C
Average district heating price [€/kWh], source: [18]	0.11
Average electricity price [€/kWh], source: [18]	0.12

Table 3 also lists the annual average price of DH and electricity in Sweden over the year of 2024 [18]. Since DH price (p_{DH}) is only slightly cheaper than electricity price (p_e) per kilowatt-hour, savings in the operational expenditure of heating (OPEX) can be reached through the heating load replacement. The annual saved OPEX can be calculated using Eq. (10), where η_{loss} represents the heat loss fraction of heating produced in the condenser over heat transportation in the integrated system. Here, we assumed fixed operating conditions of the heat pump, and the heat-pump cabinet is implemented as a lumped performance model based on the IMST-ART simulated COP. Assuming an acceptable payback period of seven years (n_{yr}=7), the justifiable capital expenditure ($CAPEX_j$) can be calculated using Eq. (11), where the annuity factor (f_a) was determined with an annual discount rate (i) of 5%.

$$OPEX_{saved} = \sum_{h=1}^{8760} [p_{DH}(1-\eta_{loss})Q_{cond} - p_e \frac{Q_{cond}}{COP_{1,tot}}] \quad (10)$$

$$CAPEX_j = \frac{OPEX_{saved}}{f_a}, \quad f_a = \frac{i}{1-(1+i)^{-n_{yr}}} \quad (11)$$

3. Experimental and Numerical Results

3.1. Experimental data and validation

Table 3 shows the results of four representative tests of the miniaturized HP under four different operating conditions, including the level of refrigerant charge and HP Fan power input ($W_{fan,HP}$). Under Test Condition 1 (2000 RPM and 137 g charge), the HP achieved the highest $\mathrm{COP}_{1,tot}$ of 3.1 and a Carnot efficiency of 41% when producing hot water at nearly 55 ºC from waste heat of 37.2ºC from the air; the heat recover ratio was measured to be 85%, suggesting that the majority of waste heat is recovered as useful hot water. Under Test Condition 2, hot water was produced at a higher temperature of 58.4ºC and the $\mathrm{COP}_{1,tot}$ became lower. Under Test Conditions 3 and 4 where the compressor speeds were higher and refrigerant charges were lower, $\mathrm{COP}_{1,tot}$ became lower, while the heat recovery ratio remains above 80%.

Table 4 Representative experimental results of heat pump performance at the standard rating condition.

Parameter	Test Condition 1	Test Condition 2	Test Condition 3	Test Condition 4
Compressor speed [RPM]	2000	2000	3500	3000
Refrigerant charge [g]	137	137	112	105
Heat source (air) temperature ($T_{a,in,HP}$/$T_{a,out,HP}$) [ºC]	37.2/27.7ºC	37.7/31.3ºC	35.0/29.2ºC	35.2/26.9ºC
Heat sink (water) temperature ($T_{w,in}$/$T_{w,out}$) [ºC]	51.0/54.7ºC	55.0/58.4ºC	49.2/54.2ºC	50.1/54.4ºC
Average water flow rate in condenser [m³/h]	0.2	0.2	0.2	0.2
Heating capacity [W]	820	783	1183	1011
HP Fan power input [W]	18.2	40.0	150.0	40.2
COP_1 [-]	3.1	2.6	2.0	2.4
Carnot efficiency [-]	41%	35%	33%	35%
Heat recovery ratio (HRR) [-]	85%	83%	82%	81%

Figure 4 shows the effects of compressor speed at the same level of refrigerant charge of 112 g and the same level of $W_{fan,HP}$ at 150 W. The heating capacity increases with compressor speed, rising from approximately 820 W at 1500 RPM to nearly 1200 W at 3500 RPM, while the evaporation temperature (T_{evap}) and $COP_{1,comp}$ decrease. This behavior suggests that the evaporator became the bottleneck when increasing the refrigerating capacity of HP, leading to significant drop in the evaporation temperature. Since the finned-tube heat exchanger (FTHE) chosen for prototyping was an off-the-shelf product which was not dedicated to this new application, we simulate improved evaporator designs with denser fins and microchannels in the following section.

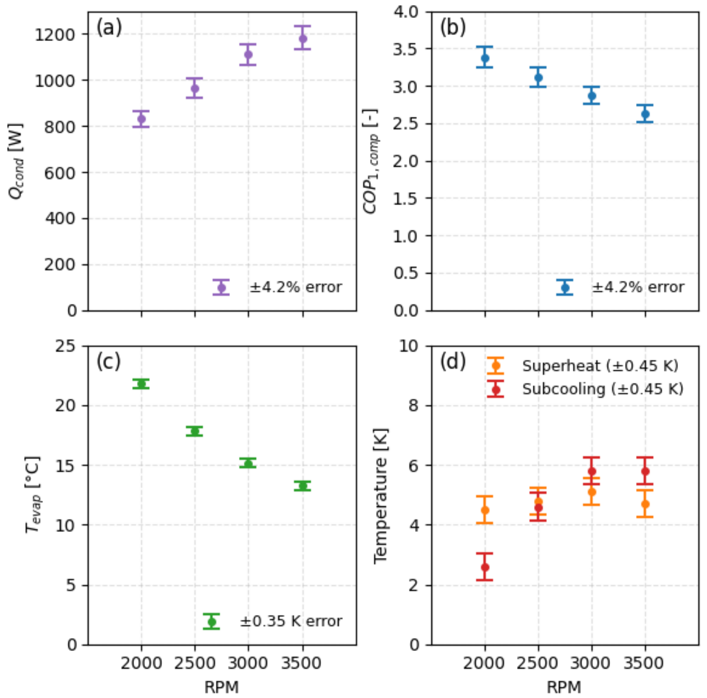

Figure 4. Experimental HP performance at varying compressor speeds (refrigerant charge = 112 g, $W_{fan,HP} \approx 150\ W$).

Figure 5 (a) and (b) compare experimental and IMST-ART simulated values of $COP_{1,comp}$ and $COP_{1,tot}$, respectively, for varying evaporator air flow rates ($V_{a,HP}$) at a fixed compressor speed (2000 RPM) and refrigerant charge (137 g). In general, the IMST-ART model shows good consistency with experimental data, indicating that the numerical model is validated for predicting HP performance. The maximum discrepancy is within 10% for a wide range of $V_{a,HP}$ between 200 and 537 m³/h. Across this flow rate range, the evaporator's UA values increased from 39 W/K to 50 W/K according to the experimental results, but the $W_{fan,HP}$ increased significantly from 10 W to 120 W. This results in a strong reduction of $COP_{1,tot}$ as shown in Figure 5 (b).

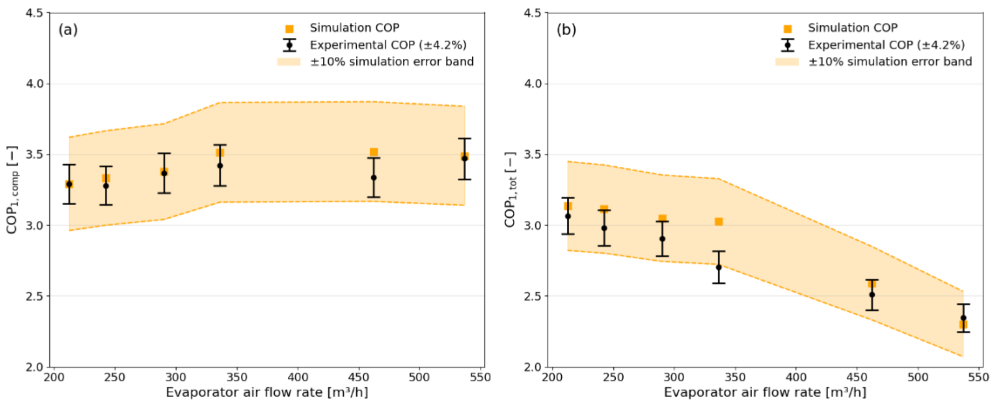

Figure 5. Experimental and numerical results of heat pump COP at varying evaporator air flow rates (RPM=2000, charge=137 g).

3.2. Numerical simulation of load-limited boundary conditions

Figure 6 shows detailed simulation results using the validated IMST-ART model when the Q_{evap} is strictly set equal to 700 W, representing a load-limited boundary condition for cooling a closed environment of the cabinet where the heat source capacity is constant and the interior temperature should be also maintained at a constant value. Increasing $V_{a,HP}$ leads to a decrease in $T_{a,in,HP}$ while $T_{a,out,HP}$ and T_{evap} remain almost unchanged. As a result, $COP_{1,comp}$ is not improved by increasing $V_{a,HP}$ and $COP_{1,tot}$ drops due to increased fan power input. The evaporator is not free to absorb more heat even if UA is increased by a higher air flow rate, because the constraint is on the load instead of heat transfer coefficient. This is different from conventional air-source HP applications where $T_{a,in,HP}$ comes from the "unlimited" ambient heat source and improving $V_{a,HP}$ simply increases the heat transfer coefficient and Q_{evap}.

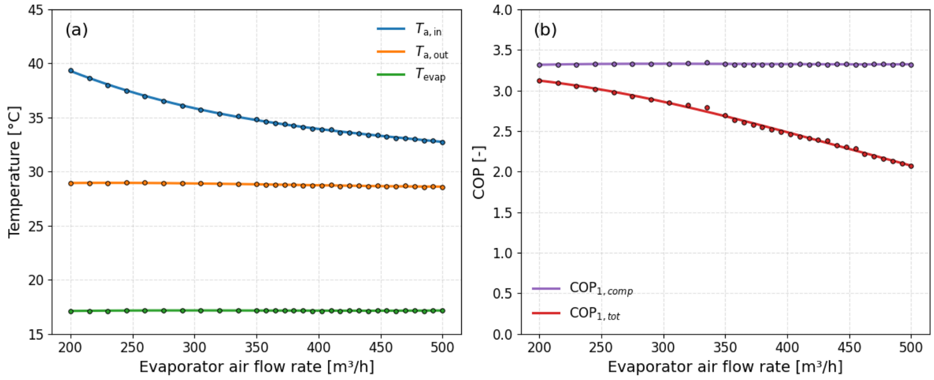

Figure 6. Numerical simulation results of heat pump performance at varying evaporator air flow rates when evaporator capacity is fixed at 700 W (Q_{evap}=700 W): (a) air and refrigerant temperatures at the evaporator; (b) $COP_{1,comp}$ and $COP_{1,tot.}$ (Compressor speed=2000 RPM; condenser water inlet/outlet temperatures=52/55ºC; Superheat/subcooling=5 K).

If we assume an ideal air flow management inside the cabinet that the air flow rate through the evaporator and BBU are the same, $T_{a,out,HP}$ is also the temperature of cold air supplied to BBU ($T_{BBU,in}$) and the outlet temperature of BBU ($T_{BBU,out}$) would become $T_{a,in,HP}$. If we need to impose higher convective cooling rates on the printed circuit boards (PCBs) inside BBU, the required air flow rate delivered by the BBU fan set usually surpasses $V_{a,HP}$ and it leads to air recirculation around BBU due to mass conservation of air. Defining a BBU-HP flow rate ratio ($r = \mathrm{m}_{a,BBU}/\mathrm{m}_{a,HP}$), we can further deduce Eqs.(6-9) as Eqs.(12-13).

$$T_{PCB,avg}(r) = T_{a,out,HP} + \frac{Q_{BBU}}{\rho_a c_{p,a} V_{a,HP}} \frac{2r-1}{2r} + Q_{BBU}/(UA_{BBU,ref}(\frac{rV_{a,HP}}{V_{BBU,ref}})^{0.8}) \tag{12}$$

$$T_j(r) = T_{a,out,HP} + \frac{Q_{BBU}}{\rho_a c_{p,a} V_{a,HP}} \frac{2r-1}{2r} + P_{hot} R_{th,j-a,ref}(\frac{V_{BBU,ref}}{rV_{a,HP}})^{0.36} \tag{13}$$

Figure 7 illustrates the calculated temperature conditions in BBU with varying values of *r* and $V_{a,HP}$, when Q_{BBU} is set as 700 W. In subfigure (a), the PCB average temperature shows almost a flat line as *r* increases, because increasing BBU fan speed only mixes some outlet air toward the inlet (bypass), raising $T_{BBU,in}$ and therefore canceling out the improved convective heat transfer coefficient when regarding the PCBs as a lump. However, hot spot temperature (T_j) is decreased as *r* increases as local junction–air convective resistance is more sensitive to air velocity. The hotspot junction temperature exhibits much stronger sensitivity to airflow than the PCB-average temperature because the local junction-to-air thermal resistance corresponds to a larger temperature rise (25–35°C). Figure 7 (b) shows that increasing $V_{a,HP}$ reduces all temperatures across the board. This figure provides a design and operational guideline when integrating HP with the cabinet. For example, if T_j must be kept below 60ºC, we can run the system with a $V_{a,HP}$ of 300 m³/h and a BBU-HP flow rate ratio of 2.

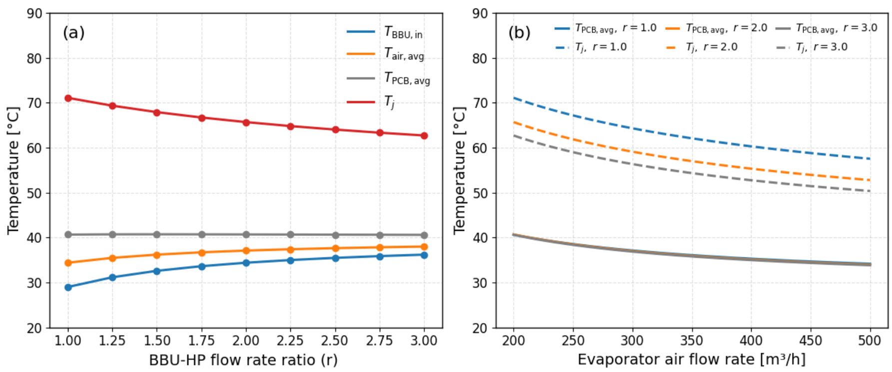

Figure 7. Calculations of heat transfer conditions inside BBU when applying HP for cooling: (a) Variations of $T_{BBU,in}$, $T_{air,avg}$, $T_{PCB,avg}$, and T_j versus increased BBU-HP flow rate ratio (*r*) when $V_{a,hp}$ is set as 200 m³/h. (b) Variations of $T_{PCB,avg}$, and Tj at varying evaporator air flow rates $V_{a,hp}$ and *r*.

4. Performance Optimization for Integration

4.1. Improvement on evaporator

As shown in Figure 4, the evaporator in the HP prototype became the bottleneck when the heating capacity was increased. To investigate improvement of HP performance by changing the evaporator, two alternative designs are evaluated using the validated IMST-ART Model: (1) a FTHE with fin spacing reduced from 4.3 mm to 2 mm; (2) a microchannel heat exchanger (MCHE) with the same frontal area as the FTHE (width × height = 315 mm × 210 mm). The analyzed MCHE is a parallel-flow type MCHE and it employs flat multi-port extruded aluminum tubes combined with louvered fins [19]; detailed design parameters can be found in Table 5.

Table 5 Design parameters of MCHE in numerical simulation

Parameter	Value
Core depth	25.4 mm
Number of ports per tube	10
Number of parallel tubes	20
Port geometry (width × height)	2 mm ×1 mm
Fin height	8 mm

Figure 8 compares the UA-values and fan power consumption of the original and improved evaporator designs under identical operating conditions. The results indicate that reducing the FTHE fin spacing from 4.3 mm to 2.0 mm increases the measured UA from 39 W/K to 53 W/K due to the higher external surface area and enhanced air-side heat transfer coefficient. The MCHE exhibits the highest UA value of 75 W/K. However, decreasing the fin spacing in the FTHE significantly increases fan power from 18.2 W to 32 W, driven by the substantial rise in air-side pressure drop. In contrast, the MCHE maintains the lowest fan power (12 W) despite its highest UA, thanks to the lower air-side resistance achieved with shorter air flow depth of the exchanger. This comparison shows that the MCHE provides the most favourable trade-off between heat transfer performance and fan power input. Therefore, this new evaporator design is used for integration analyses where HP is optimized.

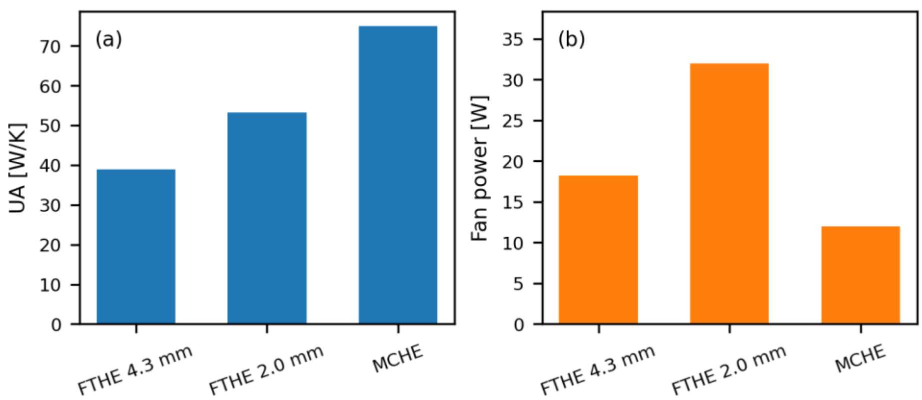

Figure 8 Comparisons of heat transfer coefficient and fan power between the original evaporator (FTHE 4.3 mm, experimental results) and improved (FTHE 2.0 mm; MCHE, numerical simulation results) evaporators in the heat pump prototype (Boundary conditions: compressor speeds=2000 RPM; $V_{a,hp}$=212 m^3/h)

4.2. Heat loss evaluation

The rooftop cabinet experiences non-negligible heat loss to the ambient air when placed in cold climates like Nordic countries. The heat loss is a plus for original functionality of the cabinet as it helps with cooling the interior area, but in heat recovery scenarios it should be reduced to maximize the recoverable amount of waste heat. Given the known cabinet geometry (1000mm×650mm×650mm), we can regard it as a lump with known surface and volume data transferring heat to ambient air which varies throughout the year. Using hourly meteorological data (T_{amb}) of Stockholm [20], the heat loss is calculated for each hour of a chosen year of 2018 and integrated for each month and the whole year, respectively. The heat loss fraction (F_{loss}) is calculated with Eq. (14), where K represents the effective thermal conductance of the heat loss. K has a baseline value of 28.5 W/K for the original cabinet without any add-on insulations, and it becomes less when adding thicker insulation (assuming a typical insulation material of $k_{ins} = 0.035\ W/(m \cdot K)$) around the cabinet. Here, we neglect solar gains as many cabinets in Stockholm are shaded on building rooftops.

$$F_{loss} = \frac{\int_0^T min(K[T_{in}(t) - T_{amb}(t)]_+, Q_{el}(t))dt}{\int_0^T Q_{el}(t)dt} \in [0,1] \tag{14}$$

Figure 9 (a) shows the monthly integrated F_{loss} for a bare cabinet when the interior temperature (T_{in}) is maintained at 15°C, 25°C, and 35°C, respectively. The high values of F_{loss} in winter months explains why many outdoor cabinets need to activate electrical heaters to keep interior temperatures above a certain threshold (e.g. 15°C) to prevent condensation and damage to the electronic equipment. Figure 9 (b) shows the annual recoverable heat fraction, which is the integral of (1-F_{loss}) throughout the year. It suggests that adding an insulation of, e.g. 50 mm, would keep the annual heat loss below 5% even if the interior temperature is kept at 35°C, which corresponds to a normal value of the average temperature of $T_{a,in,HP}$ and $T_{a,out,HP}$ shown in Figure 7.

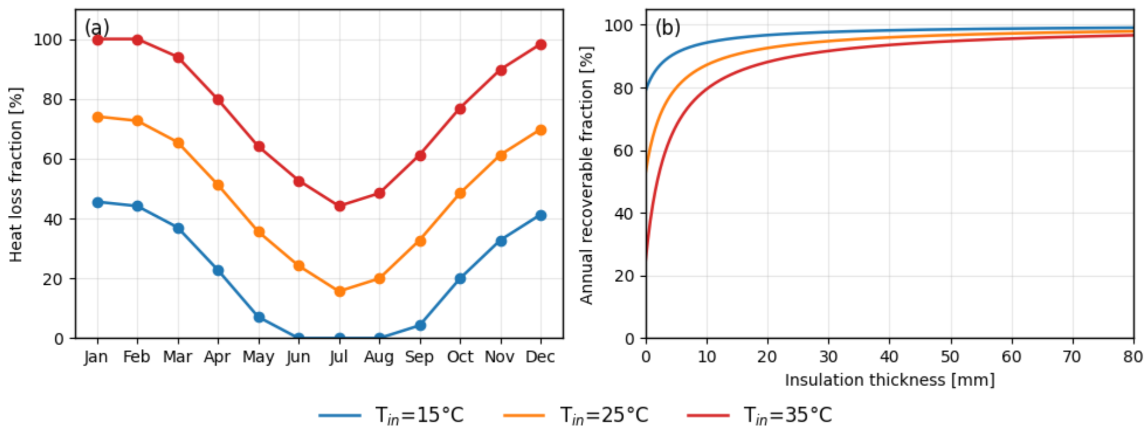

Figure 9 Heat loss calculation of cabinet on building rooftops assuming typical weather conditions in Stockholm. (a) Monthly heat loss fraction with no exterior insulation; (b) annual recoverable fraction of heat with varying insulation thickness and average internal temperatures.

The two subfigures imply the necessity to apply moderately thick insulation (40–60 mm) for retaining most of the waste heat annually while avoiding heavy jackets. By avoiding significant heat loss, insulation can also stabilize the heat source temperature to the HP.

4.3. Heating costs optimization

The economic analysis of the integration concept shown in Figure 3 can quantify how the cabinet's waste heat can be valorized. Table 6 lists the operating conditions of the renovated cabinet with HP for the economic analysis. We assumed that an insulation jacket with a thickness of 50 mm is applied to obtain a heat-recovery ratio of 95%. Due to time-constant nature of waste heat capacity in BBU, we assume the HP works at a constant condition described in Table 6 all year round. The HP delivers a heating capacity of 1.45 kW at a $COP_{1,\mathrm{tot}}$ of 3.25, simulated from the validated IMST-ART model assuming the MCHE is used. The recovered heat (Q_{evap}) is 1.2 kW after accounting the 5% of heat loss spread over the year. The waste heat comes from the BBU and heat dissipation of compressor, fans, and other electrical devices in the cabinet which are also recoverable in the renovated design. Under these conditions, the annual saving in heating costs is the value of useful hot water produced from the HP that displaces DH demands minus the electricity purchased to run the HP.

Table 6 Fixed operational conditions for heating cost saving analyses after integration

Heat pump's operational conditions		**Cabinet's heat transfer conditions**	
Condenser water inlet/outlet temperatures	52/55°C	Insulation thickness	50 mm

Condenser water flow rate	0.42 m³/h	Annual Heat recovery ratio (η_{hr})	95%
Evaporator air inlet/outlet temperatures	36.7/28.5°C	BBU-HP flow rate ratio (*r*)	2
Evaporator air flow rate [m³/h]	378	BBU inlet/outlet temperatures	36.7/32.6°C
Q_{cond}/Q_{evap}	1.45/1.20 kW	Average PCB temperature	38.3°C
$COP_{1,tot}$	3.25	Hot junction temperature	57.4 °C

Whether heating OPEX can achieve savings depends on the price difference between electricity and DH. We define the El-to-DH ratio: $\alpha = p_e/p_{\mathrm{DH}}$, to evaluate $OPEX_{saved}$ and $CAPEX_j$ over varying energy pricing conditions. It is also envisaged that the electricity and DH prices will continue increasing in Sweden, so we also evaluated p_{DH} increased by +50% and +100% in the economic analysis. Figure 10 (a) shows annual $OPEX_{saved}$ as α varies from 1 to 3.5. The three curves have the same break-even ratio of $\alpha_{\mathrm{crit}} = (1-\eta_{loss})\mathrm{COP}_{1,\mathrm{tot}} \approx 0.95 \times 3.25 \approx 3.09$. This means that the renovation to recover cabinet's waste heat is profitable whenever electricity is less than 3.09 times the DH price. Given that the α of year 2024 in Sweden is 1.06, the $OPEX_{saved}$ and $CAPEX_j$ were calculated to be 858 €/year and 10 thousand €, respectively. The components of the HP prototype cost around 2 thousand € in total, showing promising payback prospects according to the economic analysis.

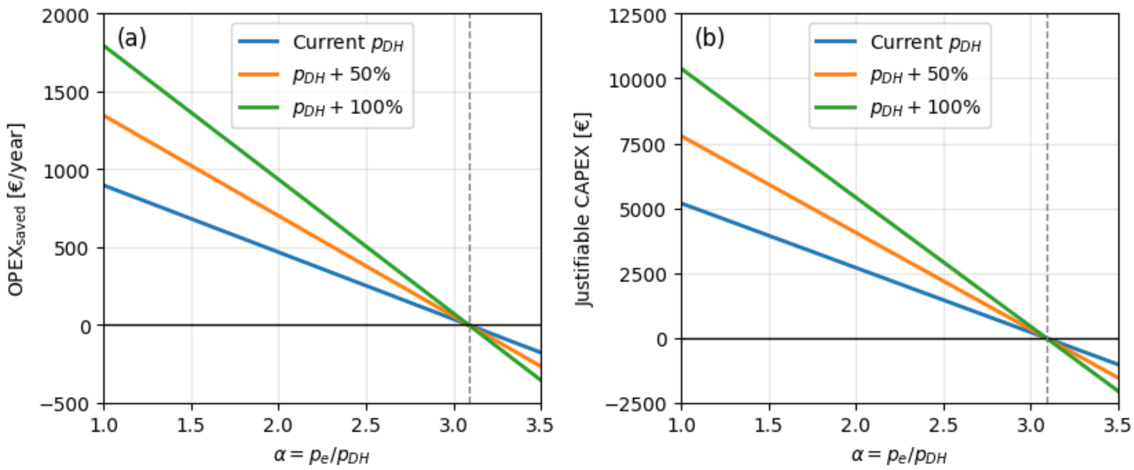

Figure 10 $OPEX_{saved}$ and $CAPEX_j$ for DHW circulation systems integrated with waste heat recovery HP.

Figure 10 also clarifies why $OPEX_{\mathrm{saved}}$ increases when both electricity and DH prices rise together. When both prices scale up by the same factor, the value of each recovered kWh of heat increases in euro by that factor, whereas the economic break-even still depends only on the price ratio $\alpha = p_e/p_{DH}$. In other words, every kilowatt-hour of DH demands avoided becomes more valuable relative to the $CAPEX$ of HP and renovation when energy becomes more expensive. Therefore, such heat recovery concepts become easier to be paid back

5. Conclusions

This study successfully designed, prototyped, and validated a novel, retrofittable "heat pump door". This miniaturized, R600a-based HP system addresses the critical gap in recovering low-grade waste heat from 5G telecommunication base stations for DHW circulation systems in buildings. Experimental validation confirmed the HP prototype's feasibility to produce DHW at 55-60°C from waste heat in the form of air inside the cabinet. The HP prototype can achieve a total COP of 3.1 and a waste heat recovery ratio of 85% while producing a heating capacity of 820 W.

A numerical HP model using IMST-ART was developed and validated by experimental data. The numerical simulations show that replacing the current evaporator with a microchannel heat exchanger (MCHE) offers a 92% higher UA-value (75 W/K) and a 34% reduction in fan power consumption. We also used a coupled simulation framework integrating the heat pump's thermodynamic model with heat transfer models of BBU and PCBs in the cabinet. The calculations show that HP integration can ensure safe cooling for BBU as the average PCB temperature and hot junction temperature can be kept below 60ºC in typical operating conditions.

In the economic analyses, we simulate the annual savings in heating OPEX by integrating an optimized HP system with DHW circulation systems. It delivers 1.45 kW of continuous heating capacity at a total COP of 3.25 while maintaining safe electronics temperatures. Per current electricity and district heating prices in Sweden, the integrated system yields 858 € in annual OPEX savings and justifies a capital expenditure (CAPEX) of 10,000 € for a 7-year payback period. This proves the economic viability of the heat recovery solution as the heat pump components only cost around 2,000 €.

Overall, this paper presents a complete, experimentally validated, and economically viable pathway for valorising the distributed waste heat from urban telecommunication infrastructure. The "heat pump door" concept centred around the miniaturized heat pump developed at our laboratory provides a scalable solution to support the sustainable transition and decarbonization of modern cities.

Acknowledgements

Swedish Energy Agency (Project number: P2022-00881 through E2B2 Programme) is thanked for providing the financial support to the research activities relating to the manuscript. Project homepage: https://www.e2b2.se/forskningsprojekti-e2b2/energitillforsel-ochdistribution/atervinning-av-varmefran-basstationer-i-mobilnatet/.

References

[1] J. Huttunen, M. Pärssinen, T. Heikkilä, O. Salmela, J. Manner, and E. Pongrácz, “Base station energy use in dense urban and suburban areas,” *IEEE Access*, vol. 11, pp. 2863–2874, 2023.
[2] A. Israr *et al.*, “Energy efficiency for 5G and beyond networks: A comprehensive review,” *Sensors*, vol. 24, no. 22, p. 7402, 2024.
[3] Huawei Technologies, *5G Power: Green Grid Slashes Costs, Emissions, and Energy Use*, Huawei, 2019.
[4] Y. Zhang, Y. Zhao, S. Dai *et al.*, “Cooling technologies for data centres and telecommunication base stations—A comprehensive review,” *Journal of Cleaner Production*, vol. 334, p. 130280, 2022.
[5] M. Lidberg, J. Åberg, and A. Mangold, “Low-temperature heating systems and the effect on district heating return temperature,” *Energies*, vol. 12, no. 24, p. 4694, 2019. *(Covers DHW temperature hygiene requirements.)*
[6] X. Zhang, Y. Li, and L. Chen, “Integrated heat-pipe and air-conditioner cooling in communication cabinets,” *Energy Reports*, vol. 7, pp. 452–461, 2021.
[7] X. Chen, X. Wang, T. Ding, and Z. Li, “Experimental analysis of an integrated cooling and heat-recovery system for data centers,” *Applied Energy*, vol. 352, p. 121875, 2023.
[8] M. Wahlroos, P. Rämä, S. Manner, and S. Syri, “Utilizing data center waste heat in district heating,” *Energy*, vol. 140, pp. 1228–1238, 2017.
[9] M. Huang, P. Rämä, and S. Syri, “Simulation of data-center waste-heat utilization in district heating networks,” *Energy*, vol. 140, 2017.
[10] IMST-ART, Institute of Energy Engineering (IIE), Universitat Politècnica de València, Valencia, Spain. [Software].
[11] F. Incropera and D. DeWitt, *Fundamentals of Heat and Mass Transfer*, Wiley, 2007.
[12] Churchill, S.W. and Bernstein, M., “A Correlating Equation for Forced Convection From Gases and Liquids to a Circular Cylinder in Crossflow,” *J. Heat Transfer*, 1977.
[13] Dell Technologies, *Dell PowerEdge HS5620 Server Thermal Testing*. Accessed: Nov. 15, 2025.[Online].
[14] Lasance, C.J.M., “The thermal resistance concept for thermal characterization of electronic packages,” *Electronics Cooling*, 1995.
[15] C.-C. Wang, “A quick overview of compact air-cooled heat sinks applicable for electronic cooling—Recent progress,” *Inventions*, vol. 2, no. 1, p. 5, Feb. 2017.
[16] Boverket. (2020). *Boverkets byggregler, BBR 29 (BFS 2019:2).* Karlskrona: Boverket.
[17] BEBO. (2016). *Slutrapport: Kartläggning av VVC-förluster i flerbostadshus.* Energimyndigheten & BeBo.
[18] Nils Holgersson Group. Fjärrvärme 2024 - nils holgersson report. Online, 2024. [Accessed: February 20, 2025].
[19] Danfoss, *Microchannel Heat Exchangers – Product Specification Guide*, D1800-C, 2019. Accessed: Feb. 2025. [Online].
[20] SMHI, “Hourly meteorological observations, Stockholm region (dry-bulb and dew-point), 2018-07-16–2018-08-01,” SMHI Open Data.